FracRisk

Reporting form for deliverables

Deliverable Number:	D5.6
Work package number:	5
Deliverable title	Report on developments for hydraulic fracturing and induced seismicity in the open-source simulator Kratos
Type	R
Dissemination Level	PU
Lead participant	CSIC
Contributing scientists and other personnel	Berta Gómez, Silvia De Simone, Jesús Carrera
Schedules delivery date from DOW	31/05/2017
Actual / forecast delivery data	30/11/2017
Comments (optional)	

Deliverable summary text:

A new code has been implemented for the assessment of the reservoir behaviour during fracking operations. This code simulates two-way Hydro-Mechanical coupling during fluid injection into porous media including pre-existing fractures that can undergo tensile or shear failure because of the pressure increase. Fractures are treated as special elements of zero-thickness and their behaviour at failure is simulated by making use of a simplified and cost-efficient procedure which considers brittle failure. The code has been validated against several benchmarks and it enables us to estimate fracture aperture and sliding during fluid injection.

Submitted	27/11/2017
Reviewed	29/11/2017
Final submission	30/11/2017

This project has received funding from the European Union's Horizon 2020 Research and Innovation programme under Grant Agreement No. 636811

Report on developments for hydraulic fracturing and induced seismicity in the open-source simulator Kratos

Berta Mª Gómez Castro, Silvia De Simone , Jesús Carrera

December 1, 2017

Contents

1 Introduction

Hydraulic fracturing operations promote the creation of new fractures and/or the reactivation of pre-existing ones (*Hubbert and Willis*, 1972). The mechanical response to pressure increase may be non trivial because of the two-way Hydro-Mechanical (HM) coupling and because of the presence of pre-existing fractures, whose conductivity changes with overpressure.

Understanding the physics of the underlying processes is of special interest because (1) the efficiency of shale gas exploitation depends on the development of the fracture network, which increases the low-permeability of the shale formation (*Rubinstein and Mahani*, 2015), (2) fracking generates great concern because reactivation of pre-existing fractures by means of shear-slip may induce seismicity, which in some cases may reach such magnitude that it is felt by local residents (*Ellsworth*, 2013), and (3) reactivation of existing faults or unstable growth may create new flow paths for the leakage of the resident or injected fluids to fresh-water aquifer (*Vengosh et al.*, 2014).

It is clear that it is necessary to properly manage fracking operations, in order to avoid undesired effects. To this end, a proper prediction of the system response is key to operation and to risk assessment. Significant advances have been achieved in recent years in the implementation of new codes for the numerical simulation of flow and deformations into porous and fractured media, as well as for the simulation of fracture aperture and propagation (see *Jing*, 2003; *Jalali and Dusseault*, 2012; *Gómez et al.*, 2016, for a review). In some cases, fractures failure and propagation are simulated by means of plastic constitutive laws, which are not appropriate for brittle failure, like in the case of shale rocks. Most of them are computationally costly which hinders their utilization for the simulation of large domain problems.

Here we present a new code that solves two-way hydro-mechanical coupling into porous media by Finite Element Method (FEM). Fractures can be included as special elements of zero-thickness and their reactivation by shear slip and/or opening is simulated with a simplified procedure that lessens the computational time without losing the correctness of the

process.

On the other hand, we do not need to develop a new code for the simulation of the reactive transport, since it will be performed by means of the existing codes Retraso-CodeBright and TOUGHREACT. These codes allow us to model the chemical interactions of the additives with the formation water and the in-situ rock minerals. Results of these simulations will be reported in Deliverable D5.9.

2 Basics of Implementation

This work focuses on the development of a new application created to simulate hydro-mechanical coupling, shear and tensile failure on porous and fractured media. We develop the HM simulator as an application named *hydromechanical application* included in the *Kratos Multi-Physics* (*Dadvand et al.*, 2010) (www.cimne.com/kratos) framework, an open source, finite element code written in C++ and developed by CIMNE (International Centre for Numerical Methods in Engineering) in Barcelona.

The choice of this framework is motivated by its flexibility to new implementations and its big and well-tested core. This core has been developed over years in order to make it suitable for the big range of applications existing in *Kratos Multi-Physics*, thus a great variety of numerical approaches are already implemented. The majority of these applications are widely tested, so this framework provides a solid base to start building a new one.

In addition to that, *Kratos Multi-Physics* is linked with GiD, an user-friendly pre- and post- processor, which simplifies the performing and analysis of simulations.

3 Hydro-Mechanical Formulation

This section summarizes the governing equations, and their corresponding FEM discretization which describes the interaction between fluid flow and a porous or fractured medium. As fractures' behaviour is different from that of the rock matrix (they may act as flow barriers or flow path and storage, they could fail causing a big opening or a shear movement,

etc.), a special formulation is needed to properly describe their discontinuity role. However, for both the fracture and the rock matrix the main unknowns are the fluid pressure p and the solid displacement $\mathbf{u}$. The numerical approach chosen to solve the resulting coupled system of equations is the fully coupled or monolithic procedure, because it is the most straightforward method since all the equations are solved simultaneously at each time step. Furthermore, this procedure is unconditionally stable and keeps second-order convergence of nonlinear iterations (*Jalali and Dusseault*, 2012). The time discretization is fully implicit, so large time steps are possible. The resulting system matrix is stored using the skyline method to reduce the storage requirement of the code. Finally, the linear system is solved by means of a LU factorization.

3.1 Continuum Medium

The combination of the fluid balance equation, together with the general form of Darcy flow, results in the groundwater flow equation for a porous medium (*Coussy*, 2004)

$$S_s \frac{\partial p}{\partial t} + \alpha \frac{\partial (\nabla \cdot \mathbf{u})}{\partial t} + \nabla \cdot \mathbf{q} + f = 0\,, \tag{1}$$

where $S_s = \frac{1}{M} = \frac{\phi}{K_f} + \frac{\alpha - \phi}{K_s}$,$M$ is the Biot's modulus, ϕ is porosity, K_f is the bulk modulus of the fluid, K_s is the bulk modulus of the solid grains,α is the Biot-Willis' coefficient defined as $\alpha = 1 - \frac{K}{K_s}$ where K is the bulk modulus of the medium, and q is Darcy flux defined as

$$\mathbf{q} = -\frac{\mathbf{k}}{\mu}(\nabla p + \rho \mathbf{g} \nabla z)\,. \tag{2}$$

If we consider the rock grains as incompressible, then $K_s = \infty$, so that $\alpha = 1$ and $S_s = \phi\beta$, where β is water compressibility. Notice that the fluid flow is coupled to the mechanical problem by means of the volumetric deformation expressed as $(\nabla \cdot \mathbf{u})$ in Eq.(1).

The FEM formulation of Eq.(1) for each element is results from appliying the Standard

Galerkin method and the Green's theorem

$$\mathbf{S}\frac{d\mathbf{p}}{dt}+\mathbf{Q}^T\frac{d\mathbf{u}}{dt}+\mathbf{H}\mathbf{p}=\mathbf{f}_p\,, \tag{3}$$

where

$$\mathbf{S}=\phi\beta\int_V \mathbf{N}^{p\,T}\mathbf{N}^p\,dV \tag{4}$$

$$\mathbf{Q}=\int_V \mathbf{B}^T\mathbf{m}\mathbf{N}^p\,dV \tag{5}$$

$$\mathbf{H}=\int_V (\nabla\mathbf{N}^p)^T\frac{\mathbf{k}}{\mu}\nabla\mathbf{N}^p\,dV \tag{6}$$

$$\mathbf{f}_p=-\int_S \mathbf{N}^{p\,T}\mathbf{q}\mathbf{n}dS+\int_V \mathbf{N}^{p\,T}f\mathbf{N}^p\,dV \tag{7}$$

and $\mathbf{N}^p$ is the matrix of shape functions which interpolates the nodal values of all state variables, $\mathbf{B}$ is a matrix composed by gradients of shape functions, $\mathbf{m}$ is a vector fulfilling the function of the identity tensor and $\mathbf{n}$ is the vector normal to the elements' surface.

On the other hand, the basic equation which describes deformation and completes with Eq. (1) the HM coupling formulation in a saturated porous media is the equilibrium of forces

$$\nabla\cdot\boldsymbol{\sigma}+\mathbf{b}=0\,, \tag{8}$$

where $\boldsymbol{\sigma}$ represents the total stress tensor and $\mathbf{b}$ is the body force vector.

This equation is coupled to pore pressure by means of the generalization of Terzaghi's

law which relates total and effective stresses ($\boldsymbol{\sigma'}$) with pressure

$$\boldsymbol{\sigma'} = \boldsymbol{\sigma} + \alpha p \mathbf{I}\,, \tag{9}$$

where $\mathbf{I}$ is the identity matrix, the sign criterion of positive tension is assumed and the Biot-Willis coefficient α is taken equal to 1.

By applying the weighted residual method and the Green's theorem, Eq. (8) at any time (for instance at t^{k+1}) can be expressed as

$$\mathbf{r}(\boldsymbol{\sigma}^{k+1}) = \int_V \mathbf{B}^T \boldsymbol{\sigma}^{k+1} dV - \mathbf{f}_u^{k+1} = \mathbf{0}\,, \tag{10}$$

where $\mathbf{r}(\boldsymbol{\sigma}^{k+1})$ is the residual corresponding to the mechanical problem, $\mathbf{B}$ is a matrix composed by gradients of shape functions and $\boldsymbol{\sigma}^{k+1}$ is the total stress vector at time t^{k+1} (notice that stresses and strains are expressed as vectors and not as tensors in FEM) and $\mathbf{f}_u^{k+1}$ includes the body force terms and the boundary condition of forces

$$\mathbf{f}_u^{k+1} = \int_V \mathbf{N}^T \mathbf{b}^{k+1} dV + \int_S \mathbf{N}^T \mathbf{t}^{k+1} dS\,. \tag{11}$$

In order to express the system in terms of the main unknowns, i.e., displacements and fluid pressure, we assume the Small Displacement Theory which relates the strain tensor ($\boldsymbol{\varepsilon}$) and displcements as follows

$$\boldsymbol{\varepsilon} = \frac{1}{2}(\nabla \mathbf{u} + (\nabla \mathbf{u})^T)\,. \tag{12}$$

Moreover, a constitutive law relating strains to effective stresses is necessary. This relationship is represented in elasticity by Hooke's law, which can be written in inremental or non-incremental formulation. Each formulation leads to different developmentof the problem due to implicit assumptions involved in each case. Both formulations have been implemented in the code as presented in the following.

3.1.1 Non-Incremental Formulation

In the non-incremental formulation the constitutive law of elasticity relates effective stresses and deformations by means of the stiffness matrix $\mathbf{D}_e$

$$\boldsymbol{\sigma}' = \mathbf{D}_e \boldsymbol{\varepsilon} \,. \tag{13}$$

Substitution of Eq. (13) into Eq. (9) and (10) yields, respectively

$$\boldsymbol{\sigma}^{k+1} + \mathbf{m} p^{k+1} = \mathbf{D}_e \boldsymbol{\varepsilon}^{k+1} \tag{14}$$

and

$$\int_V \mathbf{B}^T \mathbf{D}_e \boldsymbol{\varepsilon}^{k+1} dV - \int_V \mathbf{B}^T \mathbf{m} p^{k+1} dV - \mathbf{f}_u^{k+1} = \mathbf{0} \tag{15}$$

Note that stress is expressed as a vector in Eq. (14) so the identity matrix is replaced by the corresponding vector $\mathbf{m}$.

Equation (15) can be expressed in terms of displacements and fluid pressure (both interpoled from nodal values) using Eq. (12), which leads to

$$\mathbf{K}\mathbf{u}^{k+1} - \mathbf{Q}\mathbf{p}^{k+1} = \mathbf{f}_u^{k+1} \tag{16}$$

where

$$\mathbf{K} = \int_V \mathbf{B}^T \mathbf{D}_e \mathbf{B} dV \tag{17}$$

and

$$\mathbf{f}_u = \int_S \mathbf{N}^{u\,T} \mathbf{t} dS + \int_V \mathbf{N}^{u\,T} \rho \mathbf{g} dV \,. \tag{18}$$

This formulation considers absolute values of $\boldsymbol{\sigma}'$ and $\boldsymbol{\varepsilon}$, i.e., the values with respect to a reference state $\boldsymbol{\sigma}' = \boldsymbol{\varepsilon} = \mathbf{u} = \mathbf{0}$. Therefore, it solves problems that begin at initial condition

$\boldsymbol{\sigma}' = 0$, which means that, according to equation (9), the initial value of the normal total stresses (in compression) and the fluid pressure must be equal. If another initial stress state has to be represented, it is necessary to calculate previously the displacements of the model corresponding with such initial stress state and then proceed to calculate the displacement due to a given perturbation of the in-situ stress field. This may be inconvenient in non-linear elasticity models, because it results in a non-linear model. The inconvenience can be circumvented for large scale models by starting the initial state model with the stiffness tensor $\mathbf{D}_e$ corresponding to lithostatic and hydrostattic conditions. The advantage of this formulation is that it allows to take into consideration an initial heterogeneous strain field due to differences in the initial stress state in large scale models.

3.1.2 Incremental Formulation

In the case of incremental formulation, the constitutive law of elasticity relates increments of strains with increments of effective stresses

$$d\boldsymbol{\sigma}' = \mathbf{D}_e d\boldsymbol{\varepsilon} \tag{19}$$

or, considering time discretization,

$$\boldsymbol{\sigma}'^{k+1} - \boldsymbol{\sigma}'^{k} = \mathbf{D}_e(\boldsymbol{\varepsilon}^{k+1} - \boldsymbol{\varepsilon}^{k}). \tag{20}$$

Following the same procedure than for the non-incrmental formulation, the constituve law (Eq.(20)) is substituted into equation(9) taking into account the strain-displacement relationship expressed in equation (12), which yields

$$\boldsymbol{\sigma}^{k+1} = \boldsymbol{\sigma}^{k} - \mathbf{m}(p^{k+1} - p^{k}) + \mathbf{D}_e\mathbf{B}(\boldsymbol{u}^{k+1} - \boldsymbol{u}^{k}). \tag{21}$$

Substitution of Eq.(21) into Eq.(10) and linear interpolation of pressure and displace-

ment from nodal values lead to:

$$\mathbf{K}(\mathbf{u}^{k+1}-\mathbf{u}^{k})-\mathbf{Q}(\mathbf{p}^{k+1}-\mathbf{p}^{k})=\mathbf{f}_{u}^{k+1}-\int_{V}\mathbf{B}^{T}\boldsymbol{\sigma}^{k}\,dV\,. \tag{22}$$

Note that the equilibrium equation is expressed in terms of increments of displacements and pressures in this formulation (compare Eq.(22) with Eq.(16)).

With this formulation it is not necessary that the problem begins at $\boldsymbol{\sigma}' = 0$, since the increments consider a solution relative to an arbitrary initial stress state. For this reason, this formulation facilitates non-linear elasticity calculations, where difficulties can be circumvented by adopting a explicit formulation for tensor $\mathbf{D}_e$. However, initial strain heterogeneities due to differences in the initial stress state are difficult to simulate with this formulation. Another objection to this method is the way the boundary conditions must be applied, as they represent stress increments with respect to the initial condition.

3.2 Fractures

Fractures act as discontinuities in the displacement field because their surfaces can move one with respect to the other causing fracture opening or shear. This relative displacement is not necessarily equally divided between the two surfaces, but it can be different because of distinct acting forces, distinct stiffness in the surrounding material or differences in the boundary conditions. Moreover, these relative displacements affect the fracture permeability and therefore pressure, which in turn affect deformations. This jump in displacements across both sides of the fracture is difficult to simulate using continuity-based numerical methods as FEM. Two main approaches have been traditionally used to overcome this problem with FEM: a) methods based in lower-dimensional interface elements, b) methods using extended or enriched FEM. The first ones consist on the representation of the fracture in the mesh by means of a lower-dimensional geometry (i.e., a 1D element in a 2D domain, or a 2D element in a 3D domain) with additional intermediate nodes in order to calculate a jump in displacements between these nodes. The latter ones add local enrichment functions, which introduce additional degrees of freedom to repre-

sent displacement discontinuity across the fracture without the need of a explicit representation in the mesh. In our code fractures are represented using a method belonging to the first group. Its governing equations, FEM formulation and implementation are presented below.

3.2.1 Fracture Formulation

The fracture is implemented in the code by means of a zero-thickness, double-node interface element (*Goodman*, 1968), which means that fracture elements are polygons with area equal to zero in a 2D domain (Fig. 1 a)), whereas they are polyhedra with zero volume in a 3D domain (Fig. 1 b)).

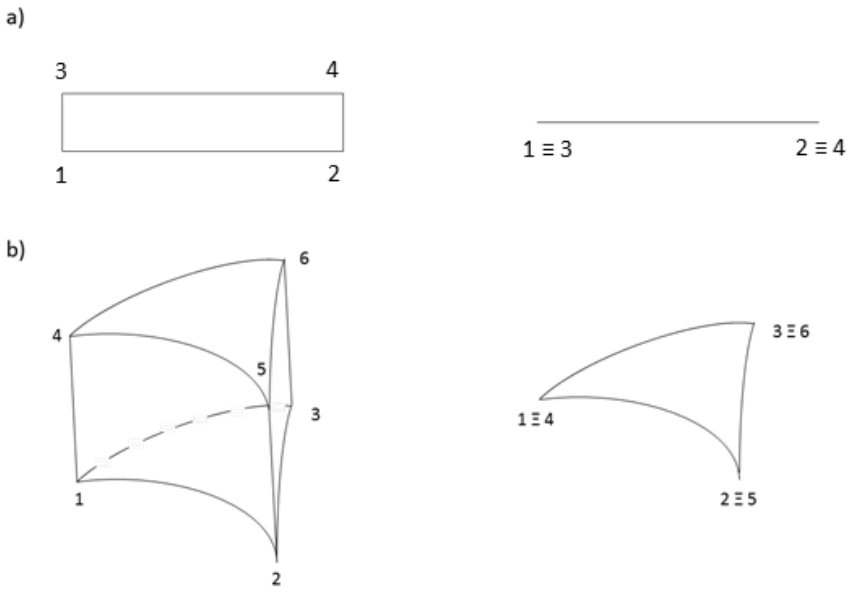

Figure 1: Interface element in (a) 2D domain and (b) 3D domain. On the left the deformed configuration is showed, whereas on the right the representation in the mesh is shown.

Fluid flow along a fracture is considered as a parallel plate model, so cubic law (*Snow*, 1969) is applied

$$\mathbf{q} = -\frac{a^2}{12\mu}\mathbf{I}(\nabla p^f + \rho \mathbf{g} \nabla z) \tag{23}$$

where a is the fracture aperture.

We assume that there is no pressure variation across the fracture, so the fluid flow equation can be written as

$$a\beta\frac{\partial p^f}{\partial t}+\alpha^f\frac{\partial a}{\partial t}+\nabla\cdot(a\mathbf{q})+f^f+\sum_{i=1}^{2}K_i\nabla h_i n_i=0\,, \tag{24}$$

where α^f can be considered equal to 1 and the last term includs the flux from the adjacent matrix. Notice that the storage term is represented by the variation of the fracture aperture and the compressibility of water stored within the fracture, as we asume a small presence of infill material in the fracture. Notice also that Eq.(24) is expressed by means of the fracture aperture a, which depends on fluid pressure. At the same time, opening or closure of the fracture affects its permeability and storage, which exhibit the two-way coupling between the mechanical and the hydraulic process. If aperture variation is appreciable, flow equation (Eq.(24)) becomes highly nonlinear, which requires full coupling to the mechanical problem and iterative solutions. However, in the hypothesis of small variations, the value of the aperture can be updated at the end of each time step.

The mechanical equations for the fracture can be formulated following the same steps presented before for the porous medium. The starting point is the momentum balance (Eq.(8)) and the relationship between fluid pressure and effective stresses (Eq.(9)). The only difference in the fracture case is that the vector of stresses has just two components, tangential and normal to the fracture, $\boldsymbol{\sigma}^f=[\tau^f,\sigma_n^f]^T$, so the vector $\mathbf{m}$ converts into $\mathbf{m}^f=[0,1]^T$ in order to consider the effect of the fluid pressure only in the direction normal to the fracture. The constituve law is expressed by increments and relates directly variations in effective stresses with variations in the relative displacement between the two faces of the fracture

$$d\boldsymbol{\sigma}'^f=\mathbf{R}^f d\,\mathbf{u}_r\,, \tag{25}$$

where $\mathbf{R}^f$ is the stiffness tensor of the fracture and $\mathbf{u}^r$ is the relative displacement vector

defined, respectively, as

$$\mathbf{R}^f = \begin{pmatrix} k_{tt} & k_{tn} \\ k_{nt} & k_{nn} \end{pmatrix} \tag{26}$$

and

$$\mathbf{u}_r = \begin{pmatrix} s \\ a \end{pmatrix} = \begin{pmatrix} u_t^+ - u_t^- \\ u_n^+ - u_n^- \end{pmatrix} \tag{27}$$

with k_{tt} and k_{nn} representing the stiffness in the tangential and normal direction respectively, and $k_{tn} = k_{nt}$ representing the dilatancy stiffness. Note that we refer to the relative displacements in the fracture, that is the difference of displacements at the two faces of the fracture. Therefore, in the vector $\mathbf{u}_r$, s represents the slip between the fracture faces and a is the fracture aperture due to the normal displacement of the fracture edges.

After applying spatial discretization, the relative displacement vector $\mathbf{u}_r$ for a fracture element is defined in terms of nodal displacements as (*Segura and Carol*, 2008b)

$$\mathbf{u}_r = \begin{pmatrix} s \\ a \end{pmatrix} = \begin{pmatrix} cos(\theta) & sin(\theta) \\ -sin(\theta) & cos(\theta) \end{pmatrix} \begin{pmatrix} N_l^u & 0 & N_r^u & 0 \\ 0 & N_l^u & 0 & N_r^u \end{pmatrix} \begin{pmatrix} -\mathbf{I}_4 & \mathbf{I}_4 \end{pmatrix} \begin{pmatrix} u_{x1} \\ u_{y1} \\ u_{x2} \\ u_{y2} \\ u_{x3} \\ u_{y3} \\ u_{x4} \\ u_{y4} \end{pmatrix} = \mathbf{T}\mathbf{N}^u\mathbf{I}_u\mathbf{u}_i \tag{28}$$

where $\mathbf{T}$ is the rotation matrix that transform the displacements in the fracture local coordinate system with inclination θ into the global coordinate system, $\mathbf{N}^u$ is a matrix of shape functions for the left and right tips of the fracture element, $\mathbf{I}_4$ is an identity matrix of dimension 4 and $\mathbf{u}_i$ is the nodal displacement vector for the generic element i.

Similarly, fluid pressure can be written for each fracture element as:

$$p_f = \begin{pmatrix} N_l^p & N_r^p \end{pmatrix} \frac{1}{2} \begin{pmatrix} \mathbf{I}_2 & \mathbf{I}_2 \end{pmatrix} \begin{pmatrix} p_1 \\ p_2 \\ p_3 \\ p_4 \end{pmatrix} = \mathbf{N}^p \frac{1}{2} \mathbf{I}_p \mathbf{p}_i \tag{29}$$

where $\mathbf{N}^p$ is the matrix of shape functions for the left and right tips of the fracture element, $\mathbf{I}_2$ is an identity matrix of dimension 2 and $\mathbf{p}_i$ is the vector of nodal pressures for the element i.

By applying this formulation to the equilibrium equation and the fluid balance equation, the governing equations for the HM problem in fractures are expressed in FEM formulation as

$$\mathbf{S}^f \frac{d\mathbf{p}}{dt} + \mathbf{Q}^{f\,T} \frac{d\mathbf{u}}{dt} + \mathbf{H}^f \mathbf{p} = \mathbf{f}_p \tag{30}$$

$$\mathbf{K}^f \mathbf{u} - \mathbf{Q}^f \mathbf{p} = \mathbf{f}_u \tag{31}$$

where

$$\mathbf{K}^f = \int_l \mathbf{I}_u^T \mathbf{N}^{u\,t} \mathbf{T}^T \mathbf{R}^f \mathbf{T} \mathbf{N}^u \mathbf{I}_u \, dl\,, \tag{32}$$

$$\mathbf{S}^f = a\beta \int_l \mathbf{I}_p^T \mathbf{N}^{p\,T} \mathbf{N}^p \mathbf{I}_p \, dl\,, \tag{33}$$

$$\mathbf{Q}^f = \int_l \mathbf{I}_u^T \mathbf{N}^{u\,T} \mathbf{T}^T \mathbf{m}^f \mathbf{N}^p \mathbf{I}_p \, dl\,, \tag{34}$$

$$\mathbf{H}^f = \int_l \mathbf{I}_p^T \frac{\partial \mathbf{N}^{pT}}{\partial l} \frac{a^3}{12\mu} \frac{\partial \mathbf{N}^p}{\partial l} \mathbf{I}_p \, dl \,. \tag{35}$$

Notice that equations(30) and (31) are similar to equations(3) and (16) respectively, but the definition of the matrixes is different. Therefore, when we consider a problem with a fracture embedded in a continuum medium, we actually solve the governing equations of the HM problem, like eq.(3) and eq.(16), but considering matrixes that are built as an assembly of the matrixes presented for the fracture and for the continuum medium. This is possible because the fracture nodes will be shared with the porous medium and their state variables will be the same.

So far we have analysed the elastic behaviour of the fracture in which displacements are small and reversible. This behaviour occurs as long as the stress tensor satisfies the equilibrium condition for tensile $\sigma_n^{'} \leq 0$ (compression positive) or shear failure $\tau \leq \mu \sigma_n^{'}$ according to the Mohr-Coulomb criterion, where τ is the tangential stress, $\sigma_n^{'}$ is the effective normal stress and μ is the friction coefficient. Once the equlibrium condition is violated, elasticity is not valid because fracture displacements become irreversible. This movement releases the amount of energy necessary to bring the system back to the equilibrium. This process is usually called fracture failure and its simulation requires the development of special numerical methods. In fragile, stiff rocks failure does not follow the classical plasticity laws, but the irreversible displacement is instantaneous at the moment the equilibrium is violated. This displacement produces a redistribution of the stresses such that the equilibrium is recovered, as expressed by

$$\tau_f + \Delta\tau = \mu(\sigma_{nf} + \Delta\sigma_n - p) \tag{36}$$

for shear failure. Aditionally,

$$\sigma_{nf} + \Delta\sigma_n - p = 0 \tag{37}$$

for tensile failure, where τ_f and σ_{nf} are the shear stress and the normal total stress of the

fracture when it fails, and $\Delta\tau$ and $\Delta\sigma_n$ represent the shear stress variation and the normal total stress variation that take place while fracture is displacing and that return the system to the equilibrium.

Our aim is to calculate the displacement field associated to this stress variation that recovers the equilibrium. To this end, we have implemented two different methods, one is based on an analytical solution and the other applies a numerical procedure, as explained in the following sections.

3.2.2 Analytical Failure Formulation: Okada Solution

Okada (1992) presented a set of closed analytical equations to calculate the variation of the internal displacement field in the medium and the variation in stresses due to a rectangular source of displacement of magnitude U over an assigned area. Three different types of rectangular sources of displacement are considered: strike displacement, dip displacement and tensile displacement. The stress variation can be written as

$$\sigma_{mn} = U[2G f_{mn} + \lambda f_{kk}\delta_{mn}], \tag{38}$$

where δ_{mn} is the Kronecker delta and f_{mn} depends only on the fracture geometry and distance to the fracture. Making use of these analytical solutions we can calculate the inverse problem, that is, given the stress variation necessary to recover equilibrium, we can calculate the resulting displacement over the failing area.

On the other hand, if the fracture is discretized in n_e elements, the total fracture displacement during failure can be calculated as the sum of the displacements in each element. In order to do that properly, it is neccesary to take into account that the displacement of each element will affect the stress state all around and will provoke displacement on other elements. The superposition of all these displacements is posssible because, although failure itself is non linear, the impact in terms of displacements and stresses, results from the response of the matrix, which is assumed to remain linear. Non-linearity is restricted to the calculation of the extent of failure, so due to the influence of one dis-

placement to the others, an iterative loop over all fracture elements is necessary to ensure that all of them are eventually in equilibrium. Therefore, recalling Eq.(36), we can write the equilibrium for element 1 as

$$\tau_{f1} - \mu\sigma'_{nf1} + \sum_{e=1}^{n_e}\left(\frac{\partial\tau_1}{\partial U_e} - \mu_d\frac{\partial\sigma'_1}{\partial U_e}\right)\Delta U_e = 0 \tag{39}$$

where τ_{f1} and σ'_{nf1} are the shear and effective normal stresses in element 1 in the moment of failure, $\partial\tau_1/\partial U_e$ and $\partial\sigma'_1/\partial U_e$ represent the stresses variation in element 1 due to the displacements in each fracture element given by the Okada solutions, and ΔU_e is the displacement at the fracture element during failure. Notice that Eq.(39) needs to be formulated for each fracture element that fails, since a variation in the stress tensor will occur in these elements due to failure.

In favor of efficiency in calculation and storage, Eq. (39) can be formulated in matrix notation

$$\begin{pmatrix}
\frac{\partial\tau_1}{\partial U_1} - \mu_d\frac{\partial\sigma'_1}{\partial U_1} & \frac{\partial\tau_1}{\partial U_2} - \mu_d\frac{\partial\sigma'_1}{\partial U_2} & \frac{\partial\tau_1}{\partial U_3} - \mu_d\frac{\partial\sigma'_1}{\partial U_3} & \cdots & \frac{\partial\tau_1}{\partial U_{e_f}} - \mu_d\frac{\partial\sigma'_1}{\partial U_{e_f}} \\
\frac{\partial\tau_2}{\partial U_1} - \mu_d\frac{\partial\sigma'_2}{\partial U_1} & \frac{\partial\tau_2}{\partial U_2} - \mu_d\frac{\partial\sigma'_2}{\partial U_2} & \frac{\partial\tau_2}{\partial U_3} - \mu_d\frac{\partial\sigma'_2}{\partial U_3} & \cdots & \frac{\partial\tau_2}{\partial U_{e_f}} - \mu_d\frac{\partial\sigma'_2}{\partial U_{e_f}} \\
\frac{\partial\tau_3}{\partial U_1} - \mu_d\frac{\partial\sigma'_3}{\partial U_1} & \frac{\partial\tau_3}{\partial U_2} - \mu_d\frac{\partial\sigma'_3}{\partial U_2} & \frac{\partial\tau_3}{\partial U_3} - \mu_d\frac{\partial\sigma'_3}{\partial U_3} & \cdots & \frac{\partial\tau_3}{\partial U_{e_f}} - \mu_d\frac{\partial\sigma'_3}{\partial U_{e_f}} \\
\vdots & \vdots & \vdots & \cdots & \vdots \\
\frac{\partial\tau_{e_f}}{\partial U_1} - \mu_d\frac{\partial\sigma'_{e_f}}{\partial U_1} & \frac{\partial\tau_{e_f}}{\partial U_2} - \mu_d\frac{\partial\sigma'_{e_f}}{\partial U_2} & \frac{\partial\tau_{e_f}}{\partial U_3} - \mu_d\frac{\partial\sigma'_{e_f}}{\partial U_3} & \cdots & \frac{\partial\tau_{e_f}}{\partial U_{e_f}} - \mu_d\frac{\partial\sigma'_{e_f}}{\partial U_{e_f}}
\end{pmatrix}
\begin{pmatrix}
\Delta U_1 \\ \Delta U_2 \\ \Delta U_3 \\ \vdots \\ \Delta U_{e_f}
\end{pmatrix} = \tag{40}$$

$$= \begin{pmatrix}
-\tau_{f1} + \mu\sigma'_{f1} \\
-\tau_{f2} + \mu\sigma'_{f2} \\
-\tau_{f3} + \mu\sigma'_{f3} \\
\vdots \\
-\tau_{fe_f} + \mu\sigma'_{fe_f}
\end{pmatrix},$$

where e_f is the number of fracture elements that fail ($e_f \leq n_e$), or in compact notation

$$\mathbf{F}_M \Delta \mathbf{U} = \boldsymbol{\sigma}_f \,. \tag{41}$$

$\mathbf{F}_M$ is called Failure Matrix, which is built and solved in the *hydromechanical application* as part of an iterative process which works as follows

1. At each time step of the simulation the equilibrium conditions are checked in every fracture element.
2. In the case in which the failure condition is met, the components of the $\mathbf{F}_M$ matrix are calculated by means of the Okada solution and the system (41) is solved for the fracture elements in failure, obtaining the displacement of each of them ΔU_e.
3. ΔU_e represents the displacement of an element along the fracture axis. Therefore, this value is transformed into the global coordinate system and the result are the two components of displacement Δu_{xe} and Δu_{ye}. For the sake of simplicity, these values are equally distributed between the upper and lower faces of the fracture element and they are imposed in the corresponding nodes.
4. The stress changes due to these imposed displacements are computed and the equilibrium in the fracture is checked again, since the displacements of the initially failed elements may have induced failure in others. If it occurs, the loop restart at step 2. If not, the simulation continues to the next time step.

This method is a efficient and straightforward manner to calculate the extension of the failure zone and the displacements originated. Usually, few iterations are needed to reach equilibrium and the analytical solution is computationally inexpensive. However, it has to be considered some drawbacks associated to the use of the analytical solutions: 1) The analytical expressions present singularities at the fault edges and 2) they are derived for a half-space, homogeneous and infinite medium so, 3) they don't take into account the boundary conditions of the model, and 4) they don't consider heterogeneities in the surrounding rock.

3.2.3 Numerical Failure Formulation: Lines of influence

In order to overcome the disadvantages of the analytical method, we also develop a numerical procedure to calculate a Failure Matrix. With this method, the Failure Matrix is specific for each model, considering its geometry, boundary conditions and the heterogeneities.

As already stated, when failure conditions are reached, the system yields with tensile aperture or shear slip, which causes a stress perturbation that recovers equilibrium (eq.(36)). This stress perturbation, and the associated displacements, is therefore the unknown of the problem.

Furthermore, the variation of the stress tensor at a point is affected not only by the local failure, but also by the failure in the surrounding, which, in the context of FEM, means that the stress field of a fracture element is affected by the failure of all the failing fracture elements. Thus, the superposition of the contribution of each fracture element should be applied, which is represented in the Failure Matrix. In order to build it, it is necessary to apply a perturbation to each fracture element to compute how this action would affect the variation of the stress state in all the rest. This procedure is performed before the simulation have started and the Failure Matrix is saved to be used, if necessary, during the simulation.

According to the principle of virtual work, the same stress variation can be provoked by the application of displacements or forces. The Failure Matrix can therefore be built by applying an unitary relative displacement or a pair of forces at the double-nodes of the fracture elements. Although both methods are equivalent, virtual forces are more suitable to implement numerically due to two main reasons: 1) applying a force only modifies the right hand side of the system matrix, whereas if a displacement is applied all the system matrix changes since displacements are state variables; 2) this method allows the nodes of the two surfaces of the fractures to displace independently, whereas the application of a relative displacement between the fracture's faces requires a initial decision about how much each face will move.

Thus, we calculate the forces T_k necessary to recover equilibrium as a result of the equi-

librium equation at each fracture element i

$$\tau_{fi} - \mu\sigma'_{nfi} + \sum_{k=a}^{n_{ed}} \left(\frac{\partial \tau_i}{\partial T_k} - \mu_d \frac{\partial \sigma'_{ni}}{\partial T_k} \right) T_k = 0\,, \tag{42}$$

where T_k is applied at each pair of double-nodes of the fracture.

The exact workflow of the implemented method is:

1. Step 0 (previous to the simulation the time loop): The Failure Matrix is built by applying fictitious unitary forces to each pair of the double-nodes (k) of the fracture and calculating the variation of stresses at each fracture element i (Fig. 2). Therefore, $\mathbf{F}_M$ has dimension ($n_e \times n_{ed}$), where n_e is the number of fracture elements and n_{ed} is the number of pairs of double-nodes.

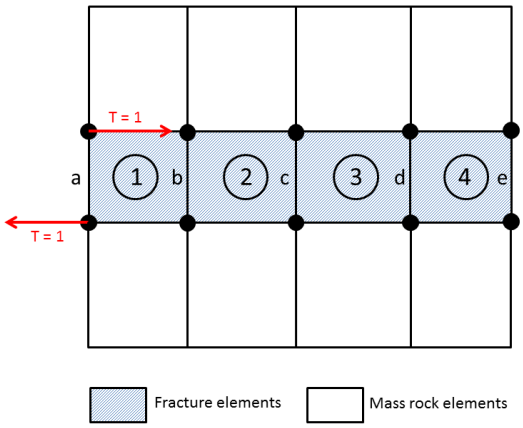

Figure 2: Schematic representation of the application of fictitious forces to a fracture embedded in a rock mass. A unitary pair of forces are applied successively at the pairs of double-nodes of the fractures (a,b,...).

2. HM simulation starts. At each time step the Mohr-Coulomb failure condition $\tau > \mu\sigma'_n$ is checked at any fracture element.

3. In case of violation of the Mohr-Coulomb criterion at one or more fracture elements, the part of the F_M corresponding to these failed elements is taken, and according to eq. (42), the following system matrix is built and solved

$$\begin{pmatrix} \frac{\partial\tau_1}{\partial T_a}-\mu_d\frac{\partial\sigma'_1}{\partial T_a} & \frac{\partial\tau_1}{\partial T_b}-\mu_d\frac{\partial\sigma'_1}{\partial T_b} & \frac{\partial\tau_1}{\partial T_c}-\mu_d\frac{\partial\sigma'_1}{\partial T_c} & \cdots & \frac{\partial\tau_1}{\partial T_{d_f}}-\mu_d\frac{\partial\sigma'_1}{\partial T_{d_f}} \\ \frac{\partial\tau_2}{\partial T_a}-\mu_d\frac{\partial\sigma'_2}{\partial T_a} & \frac{\partial\tau_2}{\partial T_b}-\mu_d\frac{\partial\sigma'_2}{\partial T_b} & \frac{\partial\tau_2}{\partial T_c}-\mu_d\frac{\partial\sigma'_2}{\partial T_c} & \cdots & \frac{\partial\tau_2}{\partial T_{d_f}}-\mu_d\frac{\partial\sigma'_2}{\partial T_{d_f}} \\ \frac{\partial\tau_3}{\partial T_a}-\mu_d\frac{\partial\sigma'_3}{\partial T_a} & \frac{\partial\tau_3}{\partial T_b}-\mu_d\frac{\partial\sigma'_3}{\partial T_b} & \frac{\partial\tau_3}{\partial T_c}-\mu_d\frac{\partial\sigma'_3}{\partial T_c} & \cdots & \frac{\partial\tau_3}{\partial T_{d_f}}-\mu_d\frac{\partial\sigma'_3}{\partial T_{d_f}} \\ \vdots & \vdots & \vdots & \cdots & \vdots \\ \frac{\partial\tau_{e_f}}{\partial T_a}-\mu_d\frac{\partial\sigma'_{e_f}}{\partial T_a} & \frac{\partial\tau_{e_f}}{\partial T_b}-\mu_d\frac{\partial\sigma'_{e_f}}{\partial T_b} & \frac{\partial\tau_{e_f}}{\partial T_c}-\mu_d\frac{\partial\sigma'_{e_f}}{\partial T_c} & \cdots & \frac{\partial\tau_{e_f}}{\partial T_{d_f}}-\mu_d\frac{\partial\sigma'_{e_f}}{\partial T_{d_f}} \end{pmatrix} \begin{pmatrix} T_a \\ T_b \\ T_c \\ \vdots \\ T_{d_f} \end{pmatrix} = \begin{pmatrix} -\tau_{f1}+\mu\sigma'_{f1} \\ -\tau_{f2}+\mu\sigma'_{f2} \\ -\tau_{f3}+\mu\sigma'_{f3} \\ \vdots \\ -\tau_{fe_f}+\mu\sigma'_{fe_f} \end{pmatrix} \tag{43}$$

   where e_f is the number of elements that fail and d_f is the number of pairs of double-nodes that fail. The solution of this system returns the forces T_k required at each double-nodes to return the system to the equilibrium.

4. The forces obtained as resolution of eq. (43) are applied to the corresponding nodes and the Failure Matrix is used again to check if the failure condition is now satisfied. In this case, the failure zone is already determined and the displacements associated are computed by the code as a result of the applied forces. If not, eq. (43) has to be solved again including the new failed elements. These virtual forces are kept throughout the simulation to acknowledge that failure is irreversible.

This numerical method is expected to be more accurate and straighforward than the analytical one based on the Okada solution because the Failure Matrix is built for each model considering its particular geometry, boundary conditions and on materials properties. The drawback is that it requires the construction of the $\mathbf{F}_M$ before starting the simulation, which slightly increases the computational time.

Both the analytical (section 3.2.2) and the numerical (section 3.2.3) methods return the

shear slip or the aperture along the fracture associated to its failure.

In the case of tensile opening this allows us to predict the aperture of a fracture during hydraulic stimulation. In the case of shear slip we can calculate the magnitude of the associated seismic event by means of $M = G\,d\,A$, where d is the displacement and A is the failing area.

4 Verification

We use some well- or less-known problems to verify the accuracy of the code and the validity of the presented formulations and methods. The different problems consider only the porous medium, only the fracture or the combination of porous medium and fractures. In the latter ones we separately check the elastic behaviour of the fracture considering only flow, only mechanical conditions or taking into account the HM coupling, besides one more test to prove the suitability of the analytical failure formulation. All the benchmarks are compared with analytical or numerical solutions and the plane strain condition is applied in all of them neglecting the gravity for fluid and solid.

4.1 Continuum Medium Benchmarks

4.1.1 Porous medium consolidation

The consolidation problem is a traditional benchmark for HM codes (*Kolditz et al.*, 2016). It considers a column of fully saturated porous medium with impermeable and constrained lateral boundaries. A compressive load is applied on the top boundary, where fluid pressure is fixed to zero. The application of the load provokes the sudden increase of pressure in the whole domain(undrained response). As time goes on, the fluid flows out of the top boundary and the column consolidates vertically until the final settlement is reached. The geometry, mesh and boundary conditions considered are showed in Figure 3 and they are based in the example provided by *Segura and Carol* (2008a). The Young's modulus is taken equal to 1000 kPa, Poison coefficient is 0.3, hydraulic conductivity is constant and equal to

1 m/d and the applied load is 10 kPa.

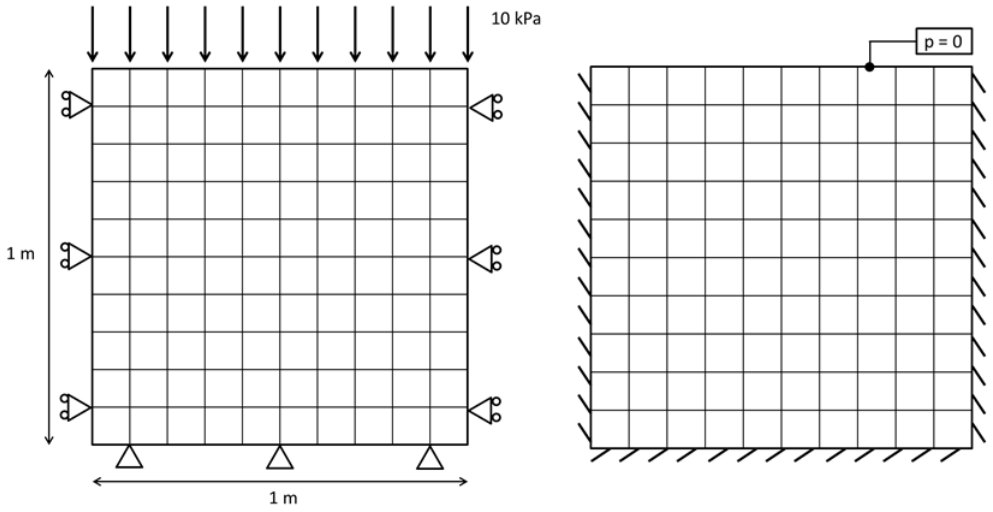

Figure 3: Geometry, mesh and mechanical (left) and hydraulic (right) boundary conditions for the porous medium consolidation problem.

This problem can be treated as a 1D problem for which there is an analytical solution (*Taylor*, 1948). Results of the numerical simulation are compared with the analytical solution (Figures 4 and 5) and demonstrate good accuracy.

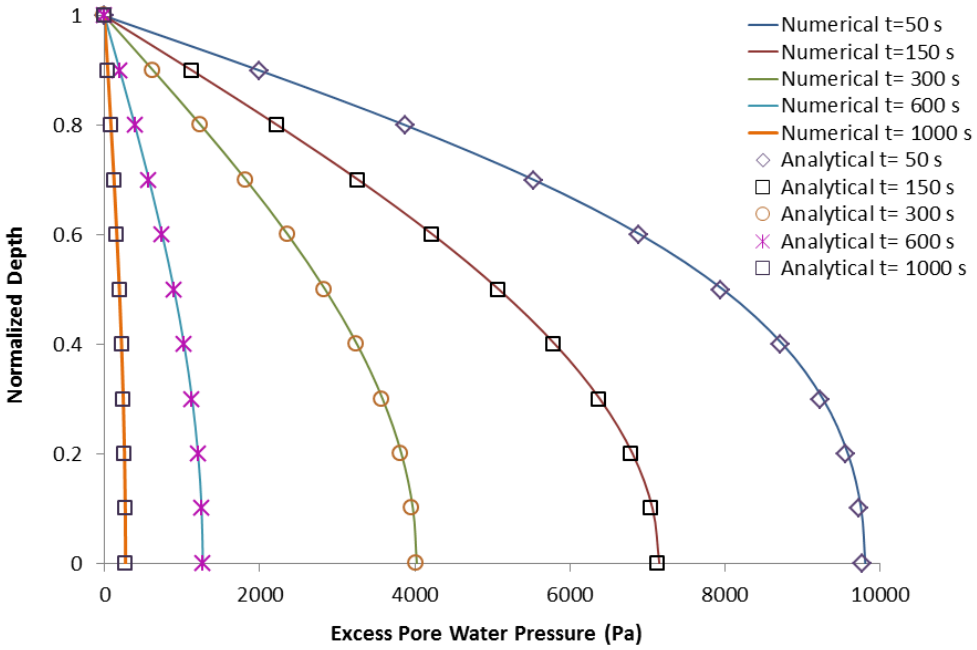

Figure 4: Results of the consolidation problem. Comparison between the pressure profile for the numerical simulation (solid line) and the analytical solution (markers) for different times.

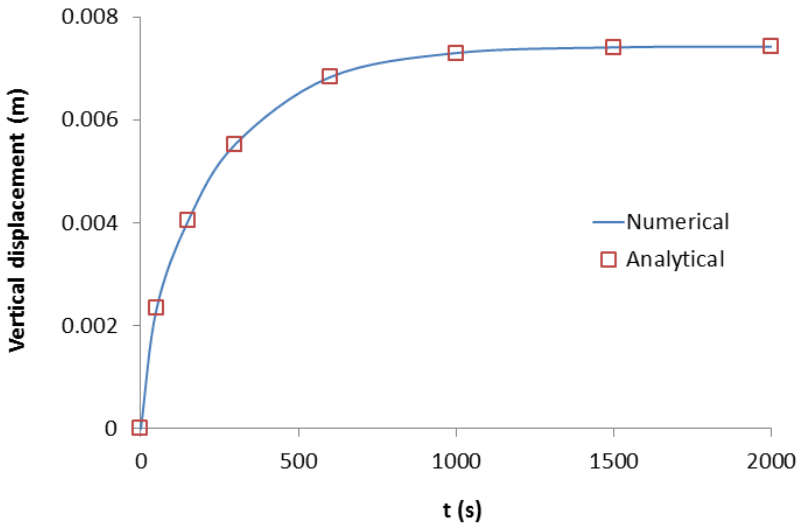

Figure 5: Results of the consolidation problem. Comparison between temporal evolution of the vertical displacement at the top of the column for the numerical simulation (solid line) and the analytical solution (markers).

4.2 Elastic Fracture Benchmarks

4.2.1 Fracture consolidation

The consolidation problem is now applied to a single horizontal fracture. The boundary conditions are based on (*Segura and Carol*, 2008a) and consist of three impermeable boundaries and one fixed-pressure boundary (Fig. 6). Analytical load of 10 kPa is applied on the top surfaceof the fracture, whereas the other boundaries are mechanically constrained. The mesh is composed by 10 linear elements and the normal fracture stiffness is equal to 20000 kPa/m whereas the tangential fracture stiffness is 1000 kPa/m. In this case, the permeability of the fracture is assumed as constant. The analytical solution in this example is the same than for the porous medium (problem of section 4.1.1) if the same consolidation coefficient is considered. To do that, fracture transmissivity has to be taken equal to $6,73x10^{-2}m^2/d$ which means that, according to the cubic law, fracture aperture is $9,85x10^{-5}m$. Comparison between the numerical results and the analytical solution (Fig. 7), proves that the fracture formulation implemented in the code works as expected.

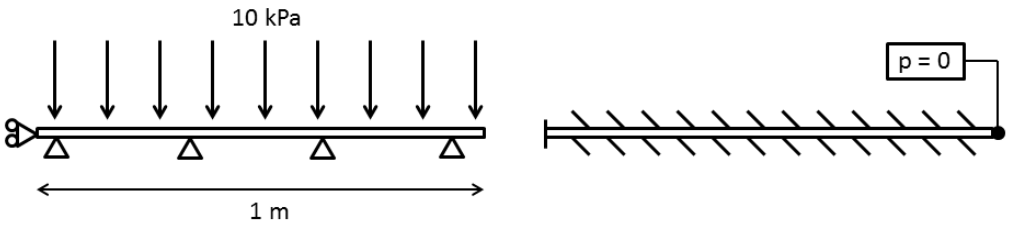

Figure 6: Geometry and mechanical (left) and hydraulic (right) boundary conditions for the fracture consolidation problem.

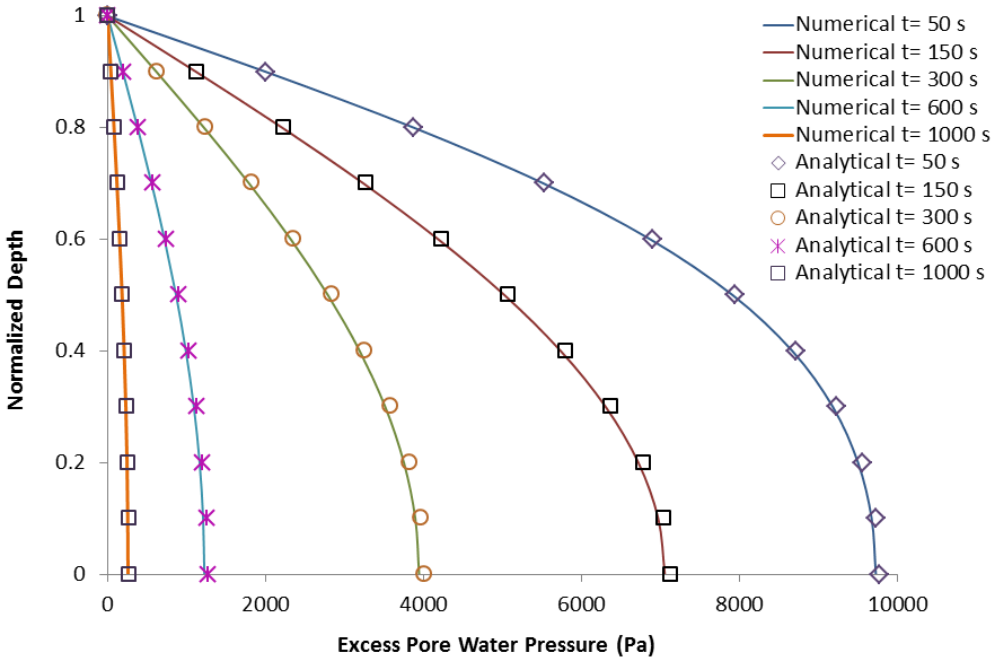

Figure 7: Results of the consolidation problem applied to the fracture. Comparison between the pressure profile for the numerical simulation (solid line) and the analytical solution (markers) for different times.

4.2.2 Flow through a fractured medium

This problem is useful to test the accuracy of the code to flow in a fractured porous medium. It is taken from *Watanabe* (2011) and consists in a 2D porous domain with an inclined fracture (45° with respect to the horizontal) embedded at the center of the domain (Fig. 8), taken from. No flow condition is applied to the top and bottom surfaces, whereas differential pressure is applied at the left and right surfaces, so that steady state flow occurs uniformly from the left to the right. The hydraulic conductivity of the fracture is constant and equal to $1x10^{-3}m/s$ which corresponds to a fracture aperture of 0.05 m. The porous medium is less conductive than the fracture with a hydraulic conductivity equal to $1x10^{-5}m/s$.

In order to compare with the analytical solution (*Strack*, 1982), which is formulated for an infinite domain, the prescribed values of pressures in the left and right boundaries of the model are derived from the analytical solution with a specific discharge $q_0 = 1x10^{-4}m/s$ (*Watanabe*, 2011). The agreement between the analytical and the numerical results of pres-

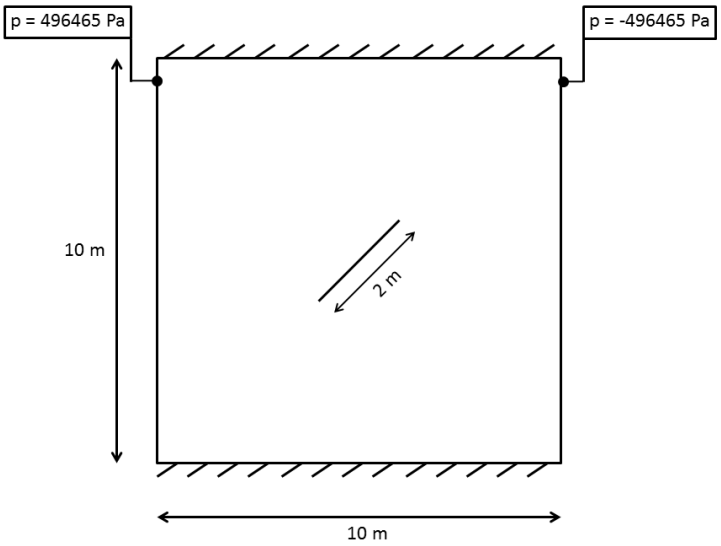

Figure 8: Geometry and hydraulic boundary conditions for the problem of flow through a fractured porous medium.

sure is presented in Fig. 9, and it is quite good despite the simplification of the fracture geometry in the simulation with respect to the geometry considered in the analytical solution (penny shape).

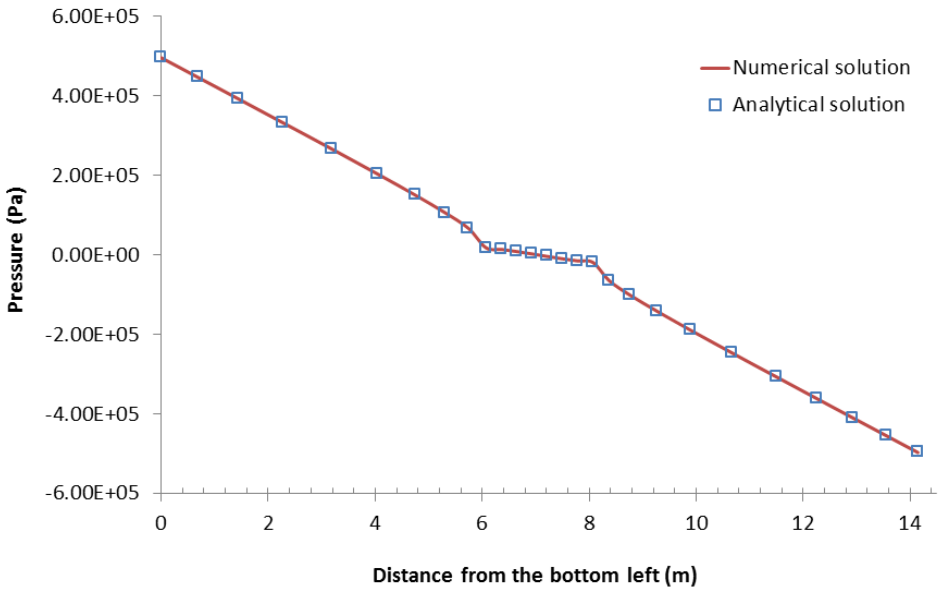

Figure 9: Results of the problem of flow through a fractured porous medium. Pressure along the diagonal of the model (from the bottom-left to the top-right) for the numerical simulation (solid line) and the analytical solution (markers).

4.2.3 Fractured rock under uniaxial load

In this benchmark only the mechanical process is simulated with a domain composed by a column of rock with an horizontal fracture in the middle under uniaxial load applied at the top. The geometry, mesh and boundary conditions are taken from *Watanabe et al.* (2012) and they are depicted in Figure 10. we assume a Young's modulus of 10 GPa, a Poisson coefficient of 0.25 and shear and normal stiffness of the fracture equal to 100 GPa/m. The applied load is equal to 1 MPa.

Due to the load on the top, the column displaces vertically. The presence of the fracture produces a jump in the vertical displacement because it has different mechanical properties than the porous matrix, as shown in Figure 11. This numerical result is compared with the analytical solution derived by *Deb and Das* (2010). The two results are in good agreement, even though they slightly diverge as long as the top boundary is approached.

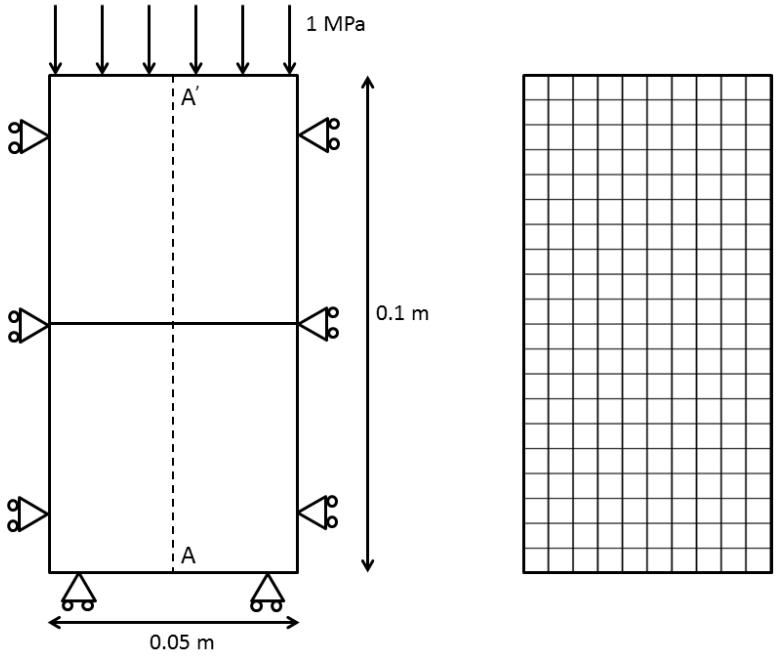

Figure 10: Geometry, mesh and mechanical boundary conditions for the problem of a fractured rock under uniaxial load.

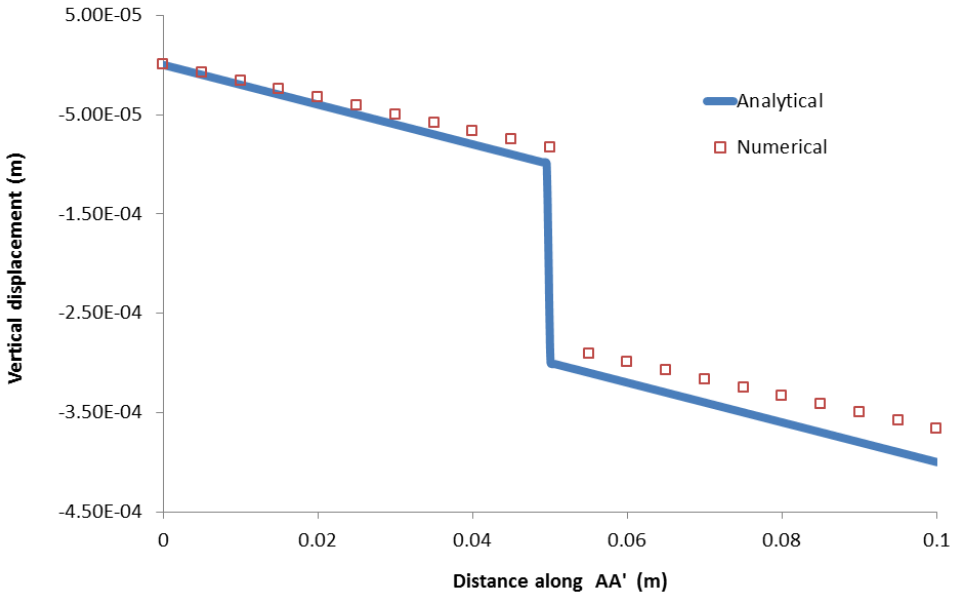

Figure 11: Results of the problem of a fractured rock under uniaxial load. Numerical (markers) and analytical (solid line) results for vertical displacement along the vertical line AA' crossing the center of the domain. Note that there is an horizontal fracture in the middle of the column.

4.2.4 Consolidation of a porous medium with a vertical fracture

This benchmark is equal to the one presented for a porous medium but a vertical fracture is included in the middle of the domain (Fig. 12). Two cases are considered: one with a constant fracture permeability and the other with variable fracture permeability, calculated by means of the cubic law. Since for these cases there are not analytical solutions, the verification is done by comparing with the numerical solutions provided by *Segura and Carol* (2008a). Moreover, we analyse the differences between the two cases and the case without fracture. The porous medium properties are the same presented in section 4.1.1, whereas the fracture has a normal stiffness equal to 20000 kPa/m and a tangential stiffness of 1000 kPa/m. The fracture transmissivity is 1 m^2/d so, according to the cubic law, fracture aperture is initially $2,4x10^{-4}m$.

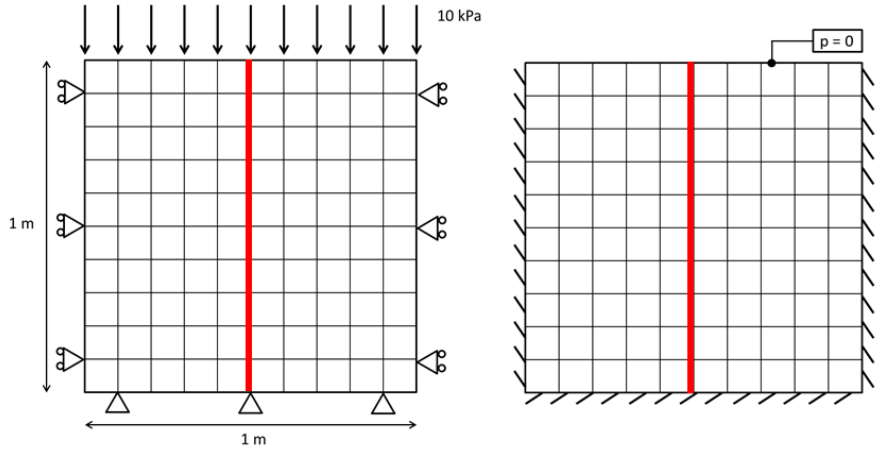

Figure 12: Geometry and mechanical (left) and hydraulic (right) boundary conditions for the consolidation problem in a porous block with a vertical fracture.

Figure 13 shows the numerical results for three consolidation cases: without fracture (only porous medium), with a constant permeability fracture and with a variable permeability. It is observed that the excess of pore water pressure reduces faster in the case with constant permeability fracture than in the case without fractures. This occurs because the fracture acts as a preferential flow path for fluid that can rapidly reach the upper boundary and get out of the system. Nevertheless, if an aperture-dependent permeability is taken into account, fluid pressure along the fracture initially reduces rapidly but, due to this reduction, the fracture aperture diminishes, which reduces drainage toward the upper bound-

ary. This effect is mainly observed in the upper part of the fracture where the excess of pressure is greater than in the case without fracture. Since the lower part of the fracture is not closed yet, this part acts as a preferential flow path and deplets the system faster than in a homogeneous porous block, reducing more the fluid pressure.

These results are reasonable and they are very similar to those obtained by *Segura and Carol* (2008a) (Fig. 14). The differences between them may be related with the residual value (the minimum value of aperture) allowed for the fracture aperture during the simulation.

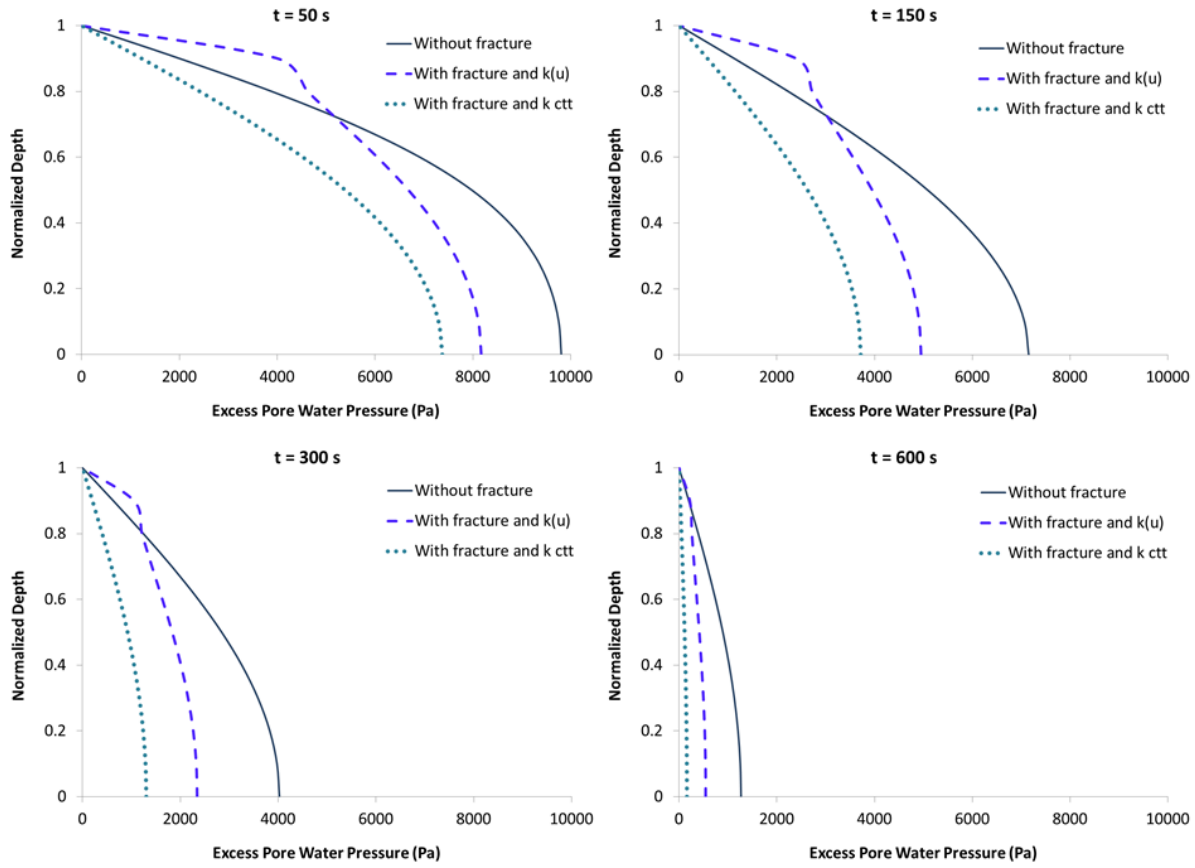

Figure 13: Results of the consolidation problem in a porous block with a vertical fracture. Pore pressure profiles along the vertical fracture for different times. The cases without fracture (solid line), with constant permeability fracture (dotted line) and with variable permeability fracture (dashed line) are compared.

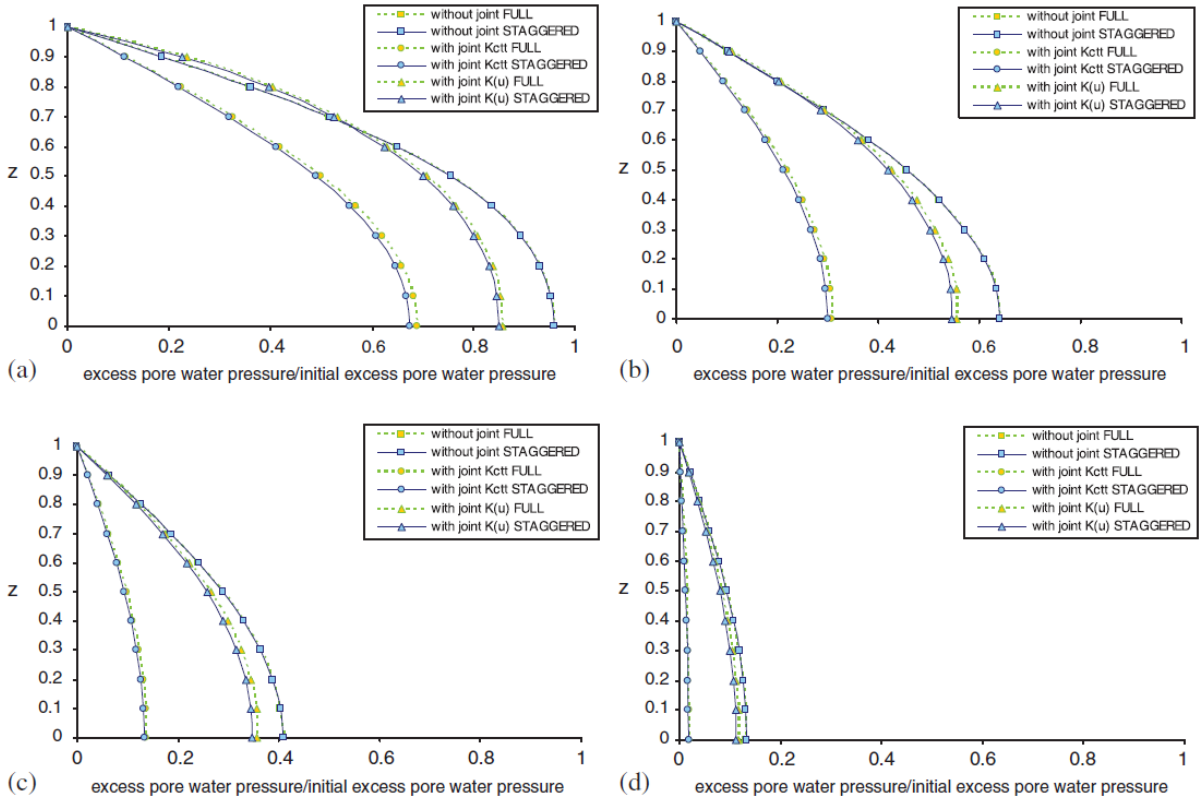

Figure 14: Results of the consolidation problem in a porous block with a vertical fracture. Fluid pressure distributions at (a) 0.0007 d, (b) 0.0021 d, (c) 0.0035 d and (d) 0.007 d. (*Segura and Carol*, 2008a).

5 Discussion and conclusions

A fully coupled HM code able to solve 2D and 3D problems has been developed with FE methodology. Two different formulations are included, each one suitable for specific cases: the Non-Incremental and the Incremental formulation. The Non-Incremental formulation requires an initial calculation of initial displacements is neccesary. Thus, this formulation allows the simulation of an initial heterogeneous strain field, that is the consequence of an initial heterogeneous stress field due to different materials and geological processes. On the other hand, the Incremental formulation is more general, since the initial condition $\sigma^{'} = 0$ is not necessary. However, heterogeneities in the initial stress field are difficult to model and the application of boundary conditions requires special care as they represent increments with respect to the initial condition. The combination of the fully coupled method (the most accurate, stable and robust (*Ferronato et al.*, 2010)) with the Incremental/Non-Incremental formulations enables the computation of a big range of different problems in a very accurate way.

In addition to that, a specifc formulation to include fractures in FEM is presented. This formulation is based on zero-thickness, double-node elements (*Goodman*, 1968). These elements allow the computation of HM processes in fractures using the same mesh used for the porous rock but adding the interface elements (one dimension lower than the domain) between faces of elements representing the porous material. Permeability may be considered constant or variablewith fracture aperture depending on whether cubic law (*Snow*, 1969) is updated or not with the fracture aperture value.

Furthermore, in order to be able to simulate fracture failure and, i.e., fracture opening during hydraulic fracturing operations or shear slip due to induced seismcity, two failure methods have been implemented, one based on the analytical solutions of *Okada* (1992) and the other numerical and based on the concept of virtual work. These methods are specific for fragile materials and they calculate failure in a more straightforward manner than other codes, which usually consider plasticity laws. Moreover, their implementation is quite easier and more direct than other methods compatible with FEM, as XFEM meth-

ods. This is because both of the implemented methods consist on the construction of a failure matrix which takes into account how the stresses in all fracture elements vary due to a perturbation (displacement or force) in only one of these elements. These variations in stresses are such that the equilibrium condition for tensile or shear in each element is recovered.

The performance of the code has been checked against several benchmarks. The good agreement of results with analytical or numerical solutions demonstrates the accuracy of the code. Nevertheless, some details of the failure methods are still being modificated and improved, so no examples of failure are shown in this document.

References

Coussy, O. (2004), *Poromechanics*, John Wiley & Sons.

Dadvand, P., R. Rossi, and E. Oñate (2010), An object-oriented environment for developing finite element codes for multi-disciplinary applications, *Archives of computational methods in engineering*, *17*(3), 253–297.

Deb, D., and K. C. Das (2010), Extended finite element method for the analysis of discontinuities in rock masses, *Geotechnical and Geological Engineering*, *28*(5), 643–659.

Ellsworth, W. L. (2013), Injection-Induced Earthquakes, *Science*, *341*(6142), 1225,942–1225,942, doi:10.1126/science.1225942.

Ferronato, M., N. Castelletto, and G. Gambolati (2010), A fully coupled 3-d mixed finite element model of biot consolidation, *Journal of Computational Physics*, *229*(12), 4813–4830.

Gómez, B., S. De Simone, V. Vilarrasa, and J. Carrera (2016), Deliverable d5.2: Review of capabilities of existing industry and research codes on the six generic focused scenarios addressed, *FracRisk Project*.

Goodman, R. (1968), A model for the mchanics of jointed rock, journal of the soil mechanics and foundation division, in *Proceedings of ASCE*.

Hubbert, M., and D. Willis (1972), Mechanics of hydraulic fracturing, *Underground Waste Management and Environmental Implications*, pp. 239–257, doi:10.1016/S0376-7361(07)53011-6.

Jalali, M. R., and M. B. Dusseault (2012), Coupling Geomechanics and Transport in Naturally Fractured Reservoirs, *46*(1), 1–26.

Jing, L. (2003), A review of techniques , advances and outstanding issues in numerical modelling for rock mechanics and rock engineering $, *39*(4), 283–353, doi:10.1016/S1365-1609(03)00013-3.

Kolditz, O., H. Shao, W. Wang, and S. Bauer (2016), *Thermo-hydro-mechanical-chemical processes in fractured porous media: modelling and benchmarking*, Springer.

Okada, Y. (1992), Internal deformation due to shear and tensile faults in a half-space, *Bulletin of the Seismological Society of America*, *82*(2), 1018–1040.

Rubinstein, J. L., and A. B. Mahani (2015), Myths and Facts on Wastewater Injection, Hydraulic Fracturing, Enhanced Oil Recovery, and Induced Seismicity, *Seismological Research Letters*, *86*(4), 1060–1067, doi:10.1785/0220150067.

Segura, J., and I. Carol (2008a), Coupled hm analysis using zero-thickness interface elements with double nodes—part ii: Verification and application, *International Journal for Numerical and Analytical Methods in Geomechanics*, *32*(18), 2103–2123.

Segura, J. M., and I. Carol (2008b), Coupled HM analysis using zero-thickness interface elements with double nodes . Part I : Theoretical model, (August), 2083–2101, doi:10.1002/nag.

Snow, D. T. (1969), Anisotropie permeability of fractured media, *Water Resources Research*, *5*(6), 1273–1289.

Strack, O. D. (1982), Assessment of effectiveness of geologic isolation systems. analytic modeling of flow in a permeable fissured medium, *Tech. rep.*, Pacific Northwest Lab., Richland, WA (USA).

Taylor, D. (1948), *Fundamentals of soil mechanics*, Chapman And Hall, Limited.; New York.

Vengosh, A., R. B. Jackson, N. Warner, T. H. Darrah, and A. Kondash (2014), A critical review of the risks to water resources from unconventional shale gas development and hydraulic fracturing in the United States, *Environmental Science and Technology*, *48*(15), 8334–8348, doi:10.1021/es405118y.

Watanabe, N. (2011), Finite element method for coupled thermo-hydro-mechanical processes in discretely fractured and non-fractured porous media.

Watanabe, N., W. Wang, J. Taron, U. J. Görke, and O. Kolditz (2012), Lower-dimensional interface elements with local enrichment: application to coupled hydro-mechanical problems in discretely fractured porous media, *International Journal for Numerical Methods in Engineering*, pp. n/a–n/a, doi:10.1002/nme.3353.